J. Fluid Mech. (1984), *vol.* 148, *pp.* 73–96
Printed in Great Britain

A turbulent bore on a beach

By I. A. SVENDSEN AND P. A. MADSEN†
Institute of Hydrodynamics and Hydraulic Engineering (ISVA), Technical University of Denmark, Building 115, DK-2800, Lyngby

(Received 1 September 1982 and in revised form 2 April 1984)

A theoretical model is developed giving a moderately detailed description of the flow in a turbulent bore, the velocity profiles, the shear stresses, the energy dissipation, etc. An analysis of the flow conditions at the toe of the turbulent front indicates significant differences from the usual description based on the finite-amplitude shallow-water equations, and it is shown that the present model gives a closer description of the actual physical conditions. Finally, numerical results are presented that illustrate how the model works, and test its validity on an example with known properties.

1. Introduction

Hydraulic jumps and bores propagating in a constant depth of water are in most respects equivalent flow phenomena. In a proper frame of reference, these flows become steady, which greatly simplifies the analysis. For the bore this means a reference frame moving with the speed of propagation of the bore.

Madsen & Svendsen (1983) (hereinafter designated I) presented a model for these cases. It included a description of the turbulence and the flow field which made it possible to describe the free-surface variation, the internal shear stresses, the energy dissipation, etc. The model was restricted to steady flow (which, in the case of a bore, corresponds to assuming a permanent form), and therefore turned out to be quite simple. In the formulation chosen, four dependent variables were used, which made it possible to satisfy depth-integrated versions of the continuity, momentum and energy equations, and in addition the momentum equation integrated over the turbulent region only. The situation is shown in figure 1.

In the present paper this model is generalized by omitting the assumption of permanent form. Hence we are now aiming at describing, for example, a bore propagating over an (arbitrarily) varying depth of water, or analysing in a fixed frame of reference a bore of permanent form propagating in a constant depth of water. Although the latter example is physically identical with the bore studied in I, the mathematical differences are quite drastic. In I the four equations required were three algebraic equations and one first-order ordinary differential equation. The same physical model for the propagating bore in a fixed frame of reference will in the following be shown to be represented by a hyperbolic system of four simultaneous partial differential equations.

If turbulence is omitted from this description, the four equations reduce to the two well-known finite-amplitude shallow-water equations (SWE), which, in fact, is the system normally used in the literature for analysing propagating bores and breaking waves. Hence the model equations derived in the following can be considered an extension of the classical SWE to include the effect of turbulence.

† Present address: Danish Hydraulic Institute, Hørsholm DK-2970, Denmark.

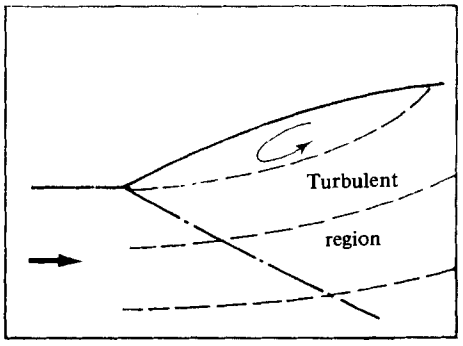

FIGURE 1. Sketch of the flow pattern in a turbulent bore: —·—, lower limit of the turbulent region; – – –, mean streamlines.

In our formulation we restrict ourselves to the turbulence generated by fronts on the free surface. The descriptions may well be extended to include bottom boundary layers, but no such attempt was made here.

As in I we assume that the horizontal lengthscale is much larger than the vertical lengthscale, which in I was shown to imply that deviations from hydrostatic pressure could be neglected in the momentum balance.

Here it is worth recalling that in the SWE the pressure is also hydrostatic, and this in combination with a uniform distribution of horizontal velocity components yields solutions for which the front side of any positive wave or bore is constantly steepening (see e.g. Peregrine 1972), in principle until a vertical face is reached.

The reason for this development can be seen by considering a constant-depth bore in a reference frame following the bore. If we assume uniform velocities and hydrostatic pressure the total momentum flux at any point of the bore is

$$M_{\mathrm{m}} = \left(\frac{Q_{\mathrm{m}}^2}{d} + \tfrac{1}{2}gd^2\right)\rho, \tag{1.1}$$

in which Q_{m} is $u_1 d_1$, u_1 being the speed of propagation of the bore and d_1 the undisturbed depth.

For a bore of permanent form this momentum flux should be constant through the bore and equal to the value at the toe, which, obviously, is not possible in (1.1) since Q is constant and only d is varying. In fact, M_{m} only attains the toe-value (namely $\rho g d_1^2(F_1^2+\frac{1}{2})$, $F_1^2 = u_1^2/gd_1$) at one other 'point', namely far behind the bore. At points in between, M_{m} is smaller, and it is in order to compensate for this momentum flux deficit that the SWE wave steepens.

This prebreaking steepening of the wave front has been studied by the method of characteristics (see e.g. Shen & Meyer (1963) for a bore, and Jeffrey (1964) and Bürger (1967) for waves), and breaking is then usually defined to occur where characteristics intercept. The time required for a given initial wave profile to develop to this point is among the results.

When the surface is approaching the vertical, however, the approximations underlying the SWE will no longer be satisfied (see e.g. Peregrine 1972). In real bores the steepening of the front will either cause the bore to become undular (the case of weak bores) or (for stronger bores) turbulent breaking will develop.

In the latter case, which we are interested in here, the water tumbling down the front face produces strongly non-uniform velocity distributions which represent an increase in momentum flux, in particular where the front is steep. If the momentum

flux is not sufficiently enhanced by the breaking, the front will steepen further, which intensifies the breaking and further increases the non-uniformity of the velocity distributions, until the front eventually becomes quasi-stable. In other words, the breaking tends to stabilize the shape of the front.

In frequency-dispersive irrotational waves (as e.g. described by the Boussinesq equations) a similar stabilization of the surface profile is obtained by the deviations from hydrostatic pressure. This mechanism was analysed closely by Peregrine (1966). To be of significance, however, this requires an appreciable curvature on the surface profile. What the above mentioned analysis in I of the pressures indicates is that in bores and hydraulic jumps this effect (apart from having the wrong sign in most of the flow region!) is far less important than the effect of the non-uniform velocity profiles caused by the breaking. Hence the stable fronts of bores and hydraulic jumps are caused, not by deviations from hydrostatic pressure (although the pressure is not quite hydrostatic) as in frequency-dispersive waves, but primarily by the turbulent breaking.

This is also consistent with the fact that if non-hydrostatic pressures become important (as in an undular bore) breaking normally ceases. In this case vanishing dissipation is then replaced by energy propagation away from the front by the trailing wave system (Benjamin & Lighthill 1954; Wilkinson & Banner 1977).

One method of obtaining numerical solutions to bores and breakers using the SWE is to replace the front by a discontinuity in the variables, supplemented by jump conditions that conserve mass and momentum across the discontinuity but dissipate energy (see e.g. Whitham 1958; Keller, Levine & Whitham 1960; Meyer & Taylor 1972).

Another approach uses a dissipative numerical scheme, usually of the type suggested by Lax & Wendroff (1960). In such schemes the shape of the front is frozen to cover a small number of computation points. Hibberd & Peregrine (1979) applied this method to a uniform bore on a beach, and Packwood (1980) studied periodic bores on a beach using measured surface variations as input at the seaward boundary.

An advantage of these methods is that they are relatively simple to use and can handle quite general problems. None of them, however, gives any information about the shape and structure of the front itself, and, as we shall see, this does influence properties such as the propagation speed.

Hence a major purpose of the present paper is to analyse the development of the front in a turbulent bore. The basic equations are formulated in §§2 and 3, the latter section describing the turbulence model. Since in addition to the four differential equations mentioned above a number of side constraints are needed, the computational procedure is outlined in §4.

The initial condition is taken to be still water over a horizontal or sloping bottom (uniformly sloping in the numerical examples), and the bore enters the region of computation by the boundary condition specified at the seaward boundary, which is placed at some distance seaward of the slope.

An important detail is then the flow at the toe of the front. A Taylor expansion is used to investigate the nature of the discontinuities occurring there. Heuristic physical arguments indicate that at the toe discontinuities occur not only in the derivatives of the dependent variable, but also in the dissipation of mean-flow energy, which becomes finite right behind the toe. The latter changes the equations at a crucial point relative to the SWE (§§6 and 7). It implies that the turbulent-bore model requires the speed of propagation of the toe (and hence that of the entire bore) to differ from the characteristic velocity at the toe. The details at the toe are compared with the flow-separation model of Longuet-Higgins (1973).

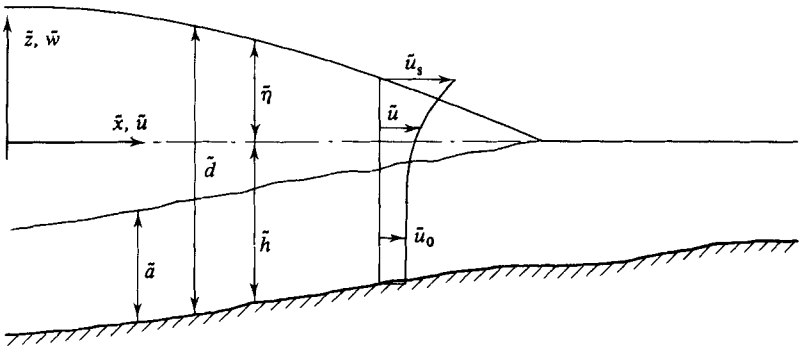

FIGURE 2. Definitions.

It is shown (§5) that, written in conservation form, the four differential equations have four real characteristic directions and so are fully hyperbolic; the numerical methods used for solution are briefly discussed in §8.

In §9 are shown numerical results for some canonical examples. The first is a uniform bore on a horizontal bottom. By using as a starting condition the solution determined in I under the assumption of steadiness, it is shown that this solution does propagate without change in form.

As another example results are given for a bore on a uniformly sloping beach.

Finally, the propagation velocities are compared with Hibberd & Peregrine's (1979) results as presented by Hibberd (1977).

The run-up which starts when the bore reaches the shoreline corresponds to a stage of the motion with no water in front of the bore. Hence the source of the surface turbulence vanishes (turbulence being now generated only in the bottom boundary layer), and the model reduces to the SWE. This part of the motion was studied extensively by Hibberd & Peregrine (1979) and Packwood (1980). In the present paper, computations stop just before the bore arrives at the shoreline, but it seems likely that the different shape and speed of the bore relative to that found by Hibberd will change the run up.

2. Assumptions and basic equations

The situation considered in shown in figure 2. The water surface is assumed at some time to be raised at the seaward boundary to a certain level and kept at that level (to produce the bore studied). The motion is described in a fixed $(\tilde{x}, \tilde{z})$-frame of reference, and the bore is assumed to propagate into quiescent water with depth $\tilde{h}(\tilde{x})$ ($\sim$ is everywhere used for dimensional variables).

In the wedge $-\tilde{h} < \tilde{z} < -\tilde{h}+\tilde{a}$ the horizontal velocities are $\tilde{u} = \tilde{u}_0(\tilde{x}, \tilde{t})$ independent of $\tilde{z}$, with $\tilde{u} = 0$ in front of the bore. In the region with turbulent flow $(-\tilde{h}+\tilde{a} < \tilde{z} < \tilde{\eta})$ we have $\tilde{u}(\tilde{x}, \tilde{z}, \tilde{t})$, where $\tilde{u}$ represents the ensemble mean velocity.

For simplicity we neglect deviations from hydrostatic pressure, which were shown in I to have a very small effect on the momentum balance of a bore in a constant depth of water. In principle, the effect of non-hydrostatic pressure can be included by a Boussinesq-type approximation. This, however, would add third-order derivative terms to the equations and complicate the computations without significant improvement in accuracy.

Consistent with this we also neglect vertical components of the Reynolds stresses,

so vertical momentum balance is not considered here. Notice that these assumptions are equivalent to assuming that the horizontal lengthscale of the motion is much larger than the vertical scale, which is known to be a dominant feature of these motions.

Finally we have neglected the contribution $\overline{u'^2}-\overline{w'^2}$ from the turbulent normal stresses in the horizontal momentum equation. Estimates based on the measurements in the literature show that the integral over depth of $\overline{u'^2}$ will at most be 10 % of the contribution from the mean velocities, so that $\overline{u'^2}-\overline{w'^2}$ will only represent a few percent correction on the total momentum (see e.g. Stive & Wind 1982).

Dimensionless variables are introduced by the definitions (using the constant velocity c_0 and the acceleration of gravity g to define the relevant scales)

$$\left.\begin{aligned} (x,z,h) &= (\tilde{x},\tilde{z},\tilde{h})\,gc_0^{-2}, & Q &= \tilde{Q}gc_0^{-3},\\ t &= \tilde{t}gc_0^{-1}, & E &= \frac{\tilde{E}g}{\rho c_0^4},\\ (u,w) &= (\tilde{u},\tilde{w})\,c_0^{-1}, & E_{\mathrm{f}} &= \frac{\tilde{E}_{\mathrm{f}}g}{\rho c_0^5},\\ & & D &= \frac{\tilde{D}}{\rho c_0^3}. \end{aligned}\right\} \tag{2.1}$$

The quantity Q is defined as

$$Q(x,t) \equiv \int_{-h}^{\eta} u\,\mathrm{d}z, \quad d(x,t) \equiv h(x)+\eta(x,t), \tag{2.2}$$

so that the equations of conservation of mass and momentum over the total depth may be written as

$$\eta_t + Q_x = 0 \tag{2.3}$$

and

$$Q_t + \left(\int_{-h}^{\eta} u^2\,\mathrm{d}z + \tfrac{1}{2}d^2\right)_x = h_x d \tag{2.4}$$

respectively, where subscript x or t means partial differentiation with respect to that variable.

Since we have a turbulent region, energy is constantly drained from the mean motion, and part of the goal is to describe the turbulence in sufficient detail to account for this.

The energy density E of the mean flow (since u is the mean velocity) per unit of horizontal area is

$$E(x,t) = \int_{-h}^{\eta} \tfrac{1}{2}u^2\,\mathrm{d}z + \tfrac{1}{2}\eta^2, \tag{2.5}$$

and the flux of energy E_{f} through any vertical section is similarly

$$E_{\mathrm{f}}(x,t) = \int_{-h}^{\eta} \tfrac{1}{2}u^3\,\mathrm{d}z + \eta Q. \tag{2.6}$$

Finally the loss D of mean energy to turbulence (equal to minus the production of turbulent energy) may be written as

$$D(x,t) = \int_{-h}^{\eta} \overline{u'w'}\frac{\partial u}{\partial z}\,\mathrm{d}z, \tag{2.7}$$

where $\overline{u'w'}$ represents the Reynolds stresses, u' and w' being the horizontal and vertical turbulent velocity fluctuations respectively, and an overbar denoting ensemble-averaging.

It may be worth mentioning here that the expression (2.7) for D represents the actual physical situation very well. The general expression for the loss of energy from the mean motion due to the work of turbulent stresses is given by $u_i\,\partial(\overline{u_i'u_j'})/\partial x_j$ (see e.g. Hinze 1959, p. 65, or 1975, p. 72). Since we assume both $\bar{w} \ll \bar{u}$ and $\partial/\partial x \ll \partial/\partial z$, this reduces to $u\,\partial\overline{u'w'}/\partial z$, which upon integration over depth yields

$$\int_a^\eta u\frac{\partial\overline{u'w'}}{\partial z}\mathrm{d}z = (u\overline{u'w'})_a^\eta - \int_a^\eta \overline{u'w'}\frac{\partial u}{\partial z}\mathrm{d}z,$$

where $(\overline{u'w'})_a = 0$ by definition. The maximum value of $(\overline{u'w'})^\eta$ can be shown to be of the same order of magnitude as the bed shear stress (the effect of which we have neglected). Further, such values only occur in the roller region. It will therefore be consistent also to neglect this term.

Using these quantities the equation for the conservation of mean energy becomes

$$E_t + E_{\mathrm{f},x} = D. \tag{2.8}$$

In the region behind the front where the turbulence covers only part of the total depth, we have for the flow in the lower, constant-velocity, region

$$u_{0,t} + u_0 u_{0,x} + \eta_x = 0, \tag{2.9}$$

which represents the conservation of momentum in that region.

Notice that although we have neglected vertical velocities it may be shown that (2.4) and (2.9) between them include the effect of transfer of horizontal momentum also by vertical entrainment of water into the turbulent region.

The integral of u^2 may be eliminated from (2.4) by means of (2.5). Doing so, the four equations (2.3), (2.4), (2.8) and (2.9) may be written in the form

with

$$\left.\begin{aligned} &\bar{V}_t + F_x(\bar{V}) = \bar{G},\\ &\bar{V} = (\eta, Q, u_0, E),\\ &F(\bar{V}) = \begin{pmatrix} Q \\ 2E - \frac{1}{2}\eta^2 + h\eta \\ \frac{1}{2}u_0^2 + \eta \\ E_{\mathrm{f}} \end{pmatrix},\\ &G = (0, \eta h_x, 0, D), \end{aligned}\right\} \tag{2.10}$$

which represents the four simultaneous partial differential equations in the unknowns η, Q, u_0 and E.

For reference it may be noticed that if we neglect the effect of turbulence the velocity will be uniform over the depth, and $D = 0$. Then the energy equation and one of the momentum equations can be derived from the other two, and the system reduces to the nonlinear shallow-water equations, which (using η and u_0 as variables) may be written

$$\eta_t + (u_0(h+\eta))_x = 0, \quad u_{0,t} + u_0 u_{0,x} + \eta_x = 0. \tag{2.11}$$

Hence the system (2.10) represents one possible extension of (2.11) that includes the effect of turbulence.

3. The turbulent-flow region

To solve (2.10) a description is required of the nature of the turbulent flow, that is $\overline{u'w'}$ in (2.7) must be related to the mean-flow properties.

The use of a depth-integrated form of the equations also makes it necessary to specify the z-variation of the horizontal velocity u in the turbulent region $a-h < z < \eta$. We use a similarity profile for $u(x,z,t)$ by writing

$$\left.\begin{aligned} \frac{u-u_0}{u_s-u_0} &= f(\sigma), \\ \text{where} \qquad \sigma &= \frac{z+h-a}{b}. \end{aligned}\right\} \tag{3.1}$$

Here $u_s = u_s(x,t)$ is u at the mean free surface, and $b = b(x,t)$ is the depth of the turbulent region (see figure 2). We need not specify $f(\sigma)$ further until later on.

For the turbulence we use a simplified k-ϵ model (see also I) where the turbulent shear stresses are given by

$$\tau = -\overline{u'w'} = \nu_t \frac{\partial u}{\partial z}, \quad \nu_t \sim \frac{k^2}{\epsilon}; \tag{3.2}$$

k is the turbulent kinetic energy defined by

$$k = \tfrac{1}{2}(\overline{u'^2} + \overline{v'^2} + \overline{w'^2}),$$

and ϵ is the dissipation of k. Following Launder & Spalding (1972), we use the relation

$$\epsilon \sim \frac{k^{\frac{3}{2}}}{b}, \quad \text{and hence} \quad \nu_t \sim k^{\frac{1}{2}} b.$$

At a fixed point, k shows a significant variation with time as the bore passes. The variation of k is described by the transport equation for k, the depth-integrated form of which was derived in I for a hydraulic jump or steady bore.

For a propagating bore described in a fixed frame of reference, the corresponding equation may be written

$$\frac{\partial}{\partial t}\int_{a-h}^{\eta} k\,\mathrm{d}z + \frac{\partial}{\partial x}\int_{a-h}^{\eta} uk\,\mathrm{d}z = \int_{a-h}^{\eta} -\overline{u'w'}\frac{\partial u}{\partial z}\,\mathrm{d}z - \int_{a-h}^{\eta} \epsilon\,\mathrm{d}z. \tag{3.3}$$

In this equation we have neglected both horizontal and vertical diffusion of turbulence. The vertical diffusion is eliminated essentially by the integration. (For a fuller discussion see I, Appendix B.) In the horizontal direction the turbulence is primarily convected with the fluid, and therefore the horizontal diffusion may also be neglected.

It is convenient to introduce the ratio Λ^2 between the dissipation and the production of k, i.e.

$$\Lambda^2 \equiv \frac{\displaystyle\int_{a-h}^{\eta} \epsilon\,\mathrm{d}z}{\displaystyle\int_{a-h}^{\eta} -\overline{u'w'}\frac{\partial u}{\partial z}\,\mathrm{d}z}, \tag{3.4}$$

so that (3.3) may be written

$$\frac{\partial}{\partial t}\int_{a-h}^{\eta} k\,\mathrm{d}z + \frac{\partial}{\partial x}\int_{a-h}^{\eta} uk\,\mathrm{d}z = (1-\Lambda^2)\int_{a-h}^{\eta} -\overline{u'w'}\frac{\partial u}{\partial z}\,\mathrm{d}z. \tag{3.5}$$

Here $\Lambda = 1$ corresponds to local equilibrium in k, which from (3.5) means k is constant following the water particles. And since particles do not follow the bore this means that the decay of the turbulence is not properly represented if $\Lambda = 1$. So to model the above-mentioned time variation of k we must, in principle, have $\Lambda \neq 1$.

In fact, in the weak bores considered here, the fluid will be moving at a much lower speed than the bore itself. In other words, on a gently sloping bottom turbulence is generated and dissipated at almost the same depth, and the terms in (3.3) may be considered independent of the bottom slope. This corresponds to using $\partial/\partial t = -c\,\partial/\partial x$ in (3.5), and this will (in a frame of reference following the front) transform (3.5) into the transport equation for a steady bore or hydraulic jump. Hence we may utilize the conclusions derived in I from that equation for the variation of the turbulence. In I it was found that the variation of k derived from the transport equation may be described with sufficient accuracy by introducing the simple approximation (here in fixed-frame variables)

$$\Lambda = \frac{c-u_0}{u_s-u_0} \tag{3.6}$$

and using

$$k = \Omega_k \Lambda^2 (u_s-u_0)^2 f'^2(\sigma), \tag{3.7}$$

where Ω_k is an empirical constant.

By substitution of (3.7) we may write

$$\nu_t = \Omega_\tau \Lambda (u_s-u_0)\, b f'(\sigma), \tag{3.8}$$

where Ω_τ is another empirical constant.

For clarity, we emphasize that in using (3.6) for Λ and (3.2) for $-\overline{u'w'}$ we do not need to specify Ω_k or to determine ϵ. In this sense and because we use the depth-integrated equations, the model is a simplified k-ϵ model. On the other hand, (3.6) does give the right variation of the balance between production and dissipation of turbulence (see I for further discussion).

Substitution of (3.1) and (3.2) into the expression (2.6) for loss of mean energy yields

$$\left.\begin{aligned} D &= -\Omega_\tau S_{10} \Lambda (u_s-u_0)^3, \\ S_{10} &\equiv \int_0^1 f'^3(\sigma)\,\mathrm{d}\sigma. \end{aligned}\right\} \tag{3.10}$$

4. Computational procedure

When (2.10) is solved numerically, we get $\bar{V} = (\eta, Q, E, u_0)$ at each time step. But to proceed from one time step to the next we must express E_f and D in terms of $\bar{V}$, which means eliminating particularly b and u_s-u_0 from the equations. In the computations this is done by the following procedure.

From (2.2) with (3.1) substituted we define

$$S_n \equiv \int_0^1 f^n(\sigma)\,\mathrm{d}\sigma, \quad n = 1,2,3, \tag{4.1a}$$

$$\phi \equiv (u_s-u_0)\, b = \frac{Q-u_0 d}{S_1}. \tag{4.1b,c}$$

Furthermore, use of (3.1) and (4.1*b*) yields

$$I_2 \equiv \int_{-h}^{\eta} u^2\,\mathrm{d}z = u_0^2 d + 2u_0 S_1 \phi + S_2 (u_s-u_0)\,\phi, \tag{4.2}$$

or
$$u_s - u_0 = \frac{I_2 - u_0^2 d - 2u_0 S_1 \phi}{S_2 \phi}. \tag{4.3}$$

But I_2 can also be expressed in terms of $\bar{V}$-components by (2.5):
$$I_2 = 2E - \eta^2. \tag{4.4}$$

Hence the computational procedure is to calculate $d = h + \eta$ and ϕ from (4.1*c*), and I_2 from (4.4). Then (4.3) yields $u_s - u_0$, and (4.1*b*) gives b. With $u_s - u_0$ and b determined, (3.10) gives D, and E_f can be found from (2.6) by substituting (3.1) into the integral, which may then be written (using (4.1)) as
$$I_3 \equiv \int_{-h}^{\eta} u^3 \, dz = u_0^3 d + 3u_0^2 \phi S_1 + 3u_0 (u_s - u_0) \phi S_2 + (u_s - u_0)^2 \phi S_3. \tag{4.5}$$

Equation (4.5) can be evaluated from the previous results, after which (2.6) gives E_f.

To summarize, the description of the flow consists of the four simultaneous differential equations (2.10). The additional relationships described above are required to eliminate the parameters brought in particularly by the turbulence model.

5. Analysis of the characteristics

It may be shown that for the constants used in the computations this system is a fully hyperbolic system, although this can only be done analytically at the toe of the turbulent front (see §6).

To proceed, we change the form of (2.10) by writing
$$\boldsymbol{F}_x(\bar{V}) = F_{i,x}(V_i) = \frac{\partial F_i}{\partial V_j} V_{j,x} = A_{ij} V_{j,x}, \tag{5.1}$$

in which $A_{ij} = A_{ij}(V_i)$ is the Jacobian matrix of $\boldsymbol{F}$. Thus (2.10) becomes
$$V_{i,t} + A_{ij} V_{j,x} = G_i, \tag{5.2}$$

and from (2.10) we find
$$A_{ij} = \begin{pmatrix} 0 & 1 & 0 & 0 \\ h-\eta & 0 & 0 & 2 \\ 1 & 0 & u_0 & 0 \\ \dfrac{\partial E_f}{\partial \eta} & \dfrac{\partial E_f}{\partial Q} & \dfrac{\partial E_f}{\partial u_0} & \dfrac{\partial E_f}{\partial E} \end{pmatrix}. \tag{5.3}$$

Using the definition (4.5), we may write (2.6) as
$$E_f = \tfrac{1}{2} I_3 + \eta Q, \tag{5.4}$$

which means that
$$\frac{\partial E_f}{\partial \bar{V}} = \begin{pmatrix} Q + \dfrac{1}{2}\dfrac{\partial I_3}{\partial \eta} \\ \eta + \dfrac{1}{2}\dfrac{\partial I_3}{\partial Q} \\ \dfrac{1}{2}\dfrac{\partial I_3}{\partial u_0} \\ \dfrac{1}{2}\dfrac{\partial I_3}{\partial E} \end{pmatrix}. \tag{5.5}$$

The derivatives of I_3 can be determined from (4.3) and from (4.5) using (4.1*b*), which yield $\partial(u_s-u_0)/\partial\bar{V}$ and

$$\frac{\partial\phi}{\partial\bar{V}}=\Big(-u_0,1,-(\eta+h),0\Big) \tag{5.6}$$

respectively. Substitution into the differentiated version of (4.5) then gives

$$\left.\begin{aligned}
\frac{\partial E_f}{\partial\eta}&=Q+\tfrac{1}{2}u_0^3-3\eta u_0+\frac{S_3}{S_1}(u_s-u_0)\Big[u_0^2-2\eta+\frac{1}{2}\frac{S_2}{S_1}u_0(u_s-u_0)\Big],\\
\frac{\partial E_f}{\partial Q}&=\eta-\tfrac{3}{2}u_0^2-\frac{1}{2}\frac{S_3}{S_2}(u_s-u_0)\Big[4u_0+\frac{S_2}{S_1}(u_s-u_0)\Big],\\
\frac{\partial E_f}{\partial u_0}&=\tfrac{1}{2}(u_s-u_0)\Big[(u_s-u_0)\,b\Big(3S_2-4\frac{S_1S_3}{S_2}\Big)+(u_s-u_0)\,\mathrm{d}\frac{S_3}{S_1}\Big],\\
\frac{\partial E_f}{\partial E}&=3u_0+2(u_s-u_0)\frac{S_3}{S_2}.
\end{aligned}\right\} \tag{5.7}$$

The characteristic directions are the four eigenvalues of A_{ij}. Since the equations are nonlinear, these directions depend on the solution, and hence vary with x and t.

6. Conditions at the toe of the front

The toe of the turbulent front is characterized by a discontinuity in some of the variables or their derivatives. This is where the dissipation starts, and D itself experiences a discontinuity at the toe of the front. This is associated with the initiation and growth of the turbulent region ($\partial b/\partial x$ and $\partial b/\partial t$ are discontinuous). Hence this point is equivalent to a shock front in the ordinary shallow-water equations.

In the following we analyse the flow properties in the neighbourhood of the toe in more detail, using an extension of a method suggested by Whitham (1974, §5.6).

In doing so it turns out that the discontinuity of D at the toe is crucial, as it changes the nature of the equations. The physical arguments for this discontinuity will be discussed in §7.

To extract the required information, we consider the flow from a frame of reference moving with the speed c of the toe of the front. Thus we introduce (ζ, T)-coordinates defined by

$$\zeta=x-ct,\quad T=t, \tag{6.1}$$

which implies that

$$\frac{\partial}{\partial T}=\frac{\partial}{\partial t}+c\frac{\partial}{\partial x},\quad \frac{\partial}{\partial\zeta}=\frac{\partial}{\partial x}, \tag{6.2}$$

with $c=c(T)$.

In the case of a bore moving into quiescent water we have in front of the bore ($\zeta>0$)

$$V_i=V_{i+}=\text{const}\quad(\zeta>0). \tag{6.3}$$

Behind the toe we expand the components of $\bar{V}$ into a Taylor series in terms of ζ (a procedure formalizing the limiting process at the toe):

$$\left.\begin{aligned}
&V_i(\zeta,T)=V_i^{(0)}(0,T)+\zeta V_i^{(1)}(0,T)+\tfrac{1}{2}\zeta^2V_i^{(2)}(0,T)+\ldots\quad(\zeta<0),\\
&\text{where}\qquad V_i^{(n)}(0,T)\equiv\Big(\frac{\partial^nV_i}{\partial\zeta^n}\Big)_{\zeta\to0-},\quad n=0,1,\ldots.
\end{aligned}\right\} \tag{6.4}$$

For physical reasons $V_i(\eta,Q,u_0,E)$ must be continuous at $\zeta=0$, so that

$$V_i(0,T)=V_{i+}\Leftrightarrow V_i^{(0)}(0,T)=V_{i+}. \tag{6.5}$$

A_{ij}, on the other hand, depends on $u_s - u_0$ (see (5.3) and (5.7)), which is discontinuous. In the expansion for A_{ij} we get

$$A_{ij} = A_{ij}^{(0)} + \zeta\left(\frac{\partial A_{ij}}{\partial V_k} V_k^{(1)} + \frac{\partial A_{ij}}{\partial \zeta}\right)_{\zeta=0-} + \ldots \quad (\zeta < 0), \tag{6.6}$$

where

$$A_{ij}(0, T) = A_{ij}^{(0)} = A_{ij}(V_{i-}). \tag{6.7}$$

For G_i we get

$$G_i = 0 \quad (\zeta > 0), \tag{6.8}$$

$$G_i = G_i^{(0)} + \zeta\left[\frac{\partial G_i}{\partial V_k} V_k^{(1)} + \frac{\partial G_i}{\partial \zeta}\right]_{\zeta=0-} + \ldots \quad (\zeta < 0). \tag{6.9}$$

When the expansions are substituted into (5.2) and terms collected corresponding to equal powers of ζ, we get for the first two orders of approximation

$$\zeta^0: \quad (A_{ij}^{(0)} - c\delta_{ij})\, V_j^{(1)} = G_i^{(0)}, \tag{6.10}$$

$$\zeta^1: \quad \frac{\mathrm{d}V_i^{(1)}}{\mathrm{d}T} + (A_{ij}^{(0)} - c\delta_{ij})\, V_j^{(2)} + V_i^{(1)}\left[\frac{\partial A_{ij}}{\partial V_k} V_k^{(1)} + \frac{\partial A_{ij}}{\partial \zeta}\right]_{\zeta=0} = \left[\frac{\partial G_i}{\partial V_k} V_k^{(1)} + \frac{\partial G_i}{\partial \zeta}\right]_{\zeta=0}. \tag{6.11}$$

Here (6.10) represents a system of algebraic equations for $V_j^{(1)}$, the first-order derivatives of V_j at the toe. In the special case considered by Whitham, $G_i^{(0)} = 0$, corresponding to G_i continuous at the toe (as e.g. in the nonlinear shallow-water equations). Obviously this implies that solutions for $V_j^{(1)}$ only exist provided that

$$|A_{ij}^{(0)} - c\delta_{ij}| = 0, \tag{6.12}$$

i.e. c is one of the eigenvalues of $A_{ij}^{(0)}$. Then, however, there are infinitely many linearly dependent solutions for $V_j^{(1)}$, which may be written σL_j, where L_j is the right eigenvector of $A_{ij}^{(0)}$.

Since $G_i^{(0)} = 0$ implies $u_s - u_0 = 0$ according to (3.10), and $\zeta = 0$ implies $V_i = 0$ in $A_{ij}^{(0)}$, the solutions to (6.12) correspond to solutions to the linearized version of (5.2) (i.e. the equations corresponding to the wave equation in the shallow-water case).

Multiplying (6.11) by the left eigenvector l_i of A_{ij} and utilizing that c is given by (6.12), Whitham eliminates $V_j^{(2)}$ from (6.11), which yields an equation of the form

$$l_i L_i \frac{\mathrm{d}\sigma}{\mathrm{d}T} + a_1\sigma + a_2\sigma^2 = 0. \tag{6.13}$$

This is a Bernoulli equation describing the rate at which the derivatives $V_i^{(1)}$ at the toe change as the bore propagates. A similar equation was derived by a slightly different approach by Jeffrey & Mvungi (1980). Notice that, if (5.2) is truly linear, i.e. A_{ij} is independent of V_i, then (6.11) yields $\mathrm{d}V_i^{(1)}/\mathrm{d}T = 0$, i.e. all solutions propagate without change of shape (in accordance with the abovementioned wave equation for the shallow-water case).

In the present model, however, we find

$$G_i^{(0)} = (0, 0, 0, D^{(0)}), \tag{6.14}$$

where $D^{(0)}$ is the dissipation at $\zeta = 0-$. $D^{(0)}$ as determined from (3.10) is shown below to be non-zero.

Hence solutions to (6.10) only exist provided that c differs from the eigenvalues of A_{ij} (which are at the same time the slope of the characteristics in the (x, t)-plane). Physically, this means that the toe propagates at a speed c that depends on the rate of change of η, Q, u_0 and E immediately behind the bore toe and is different from the characteristic speed. On the other hand, this implies that for each value of c satisfying this condition there is one set of solutions for $V_j^{(1)}$.

In more detail, the case we consider corresponds to

$$\left.\begin{aligned} &\eta^{(0)} = Q^{(0)} = u^{(0)} = E^{(0)} = 0, \\ &d^{(0)} = h, \quad \phi^{(0)} = \frac{Q^{(0)} - u^{(0)} d^{(0)}}{S_1} = 0 \end{aligned}\right\} \quad \text{at} \quad \zeta = 0, \tag{6.15}$$

which substituted into (5.7) and (5.3) yields

$$(A_{ij}^{(0)} - c\delta_{ij}) = \begin{pmatrix} -c & 1 & 0 & 0 \\ h & -c & 0 & 2 \\ 1 & 0 & -c & 0 \\ 0 & -\frac{1}{2}\frac{S_3}{S_1}(u_s - u_0)^{(0)2} & \frac{1}{2}h\frac{S_3}{S_1}(u_s - u_0)^{(0)2} & 2(u_s - u_0)^{(0)}\frac{S_3}{S_2} - c \end{pmatrix}, \tag{6.16}$$

where $(u_s - u_0)^{(0)}$ is $u_s - u_0$ taken at $\zeta = 0$, and S_n is given by (4.1*a*).

When this is used in (6.10) together with (6.14), the first three equations of (6.10) may be solved directly to yield

$$Q^{(1)} = c\eta^{(1)}, \tag{6.17}$$

$$E^{(1)} = \tfrac{1}{2}(c^2 - h)\,\eta^{(1)}, \tag{6.18}$$

$$u_0^{(1)} = \eta^{(1)}/c. \tag{6.19}$$

The last equation of (6.10) then gives

$$\eta^{(1)} = 2\frac{D^{(0)}}{c^3}\frac{c^2}{c^2 - h}\left(-\frac{S_3}{S_1}\frac{(u_s - u_0)^{(0)2}}{c^2} + 2\frac{(u_s - u_0)^{(0)}}{c}\frac{S_3}{S_2} - 1\right)^{-1}. \tag{6.20}$$

Together these equations express $V_i^{(1)}$ in terms of c, but may also be considered as relations giving c in terms of $\eta^{(1)}$ or other components of $V_i^{(1)}$.

This is in fact how the results are used in the computations. It turns out that the computations are stable if c is determined from (6.17) and unstable if (6.20) is used.

Notice that the solution found for $V_i^{(1)}$ is a locally constant-depth solution as it does not depend explicitly on the bed slope h_x.

The second approximation given by (6.10) shows that (since $V_i^{(2)}$ cannot be eliminated as in the homogeneous case) the rate at which $V_i^{(1)}$ changes with time depends not only on the first derivatives of V_i, but also on the curvature $V_i^{(2)}$ of V_i. Hence determination from (6.11) and higher-order approximations of the time variation of V_i at the toe becomes rather complicated in the case $G_i^{(0)} \neq 0$.

Equation (6.11) and the higher-order equations may, however, also be considered from a different point of view. Since the turbulence is stabilizing the front, the possibility exists of constant-form solutions for the front; or, more likely, solutions showing similarity (in the neighbourhood of the toe) in suitably chosen variables as the front propagates towards the shore. Such a solution would be characterized by $\mathrm{d}^n/\mathrm{d}T^n = 0$ or a value determined by the similarity relations. Thus (6.11) (and higher-order approximations) turn into algebraic equations in $V^{(n)}$, which are equations for the Taylor coefficients of a solution deforming to fit the similarity relations.

The value of $u_s - u_0$ at the toe may be determined from the equations in §4 by

Taylor expansion of all variables. Thus (4.1*c*), (4.3) and (4.4) yield with (6.17)–(6.19) substituted

$$\left.\begin{aligned} \phi^{(0)} = 0, \quad \phi^{(1)} &= \frac{c^2-h}{c\,S_1}\eta^{(1)}, \\ (u_s-u_0)^{(0)} &= \frac{I_2^{(1)}}{S_2}\phi^{(1)}, \\ I_2^{(1)} &= (c^2-h)\,\eta^{(1)}, \end{aligned}\right\} \tag{6.21}$$

so that

$$(u_s-u_0)^{(0)} = c\frac{S_1}{S_2}. \tag{6.22}$$

Substitution of this into (6.20) then gives

$$\left.\begin{aligned} \eta^{(1)} &= 2\frac{D^{(0)}}{c^3(S_5-1)}\frac{c^2}{c^2-h}, \\ \text{with} \qquad S_5 &= \frac{S_1 S_3}{S_2^2}. \end{aligned}\right\} \tag{6.23}$$

In fact, we may also at the toe determine the eigenvalues of A_{ij} (that is of $A_{ij}^{(0)}$) explicitly. We substitute (6.22) into $A_{ij}^{(0)}$ and set $\det(A_{ij}^{(0)}-\lambda_A\delta_{ij}) = 0$, which yields the eigenvalues λ_A:

$$\lambda_A = \left\{\begin{matrix} \pm h^{\frac{1}{2}}, \\ c(S_5 \pm (S_5(S_5-1))^{\frac{1}{2}}). \end{matrix}\right\} \tag{6.24}$$

This confirms analytically that two of the eigenvalues behind the toe are equal to the eigenvalues in the inviscid flow in front of the toe.

Figure 3 shows in an (x,t)-diagram the position at the front of all four eigenvalues. The case is $c/h^{\frac{1}{2}} = 2$ and $f(\sigma)$ equal to the cubic used in §9. c is here the velocity of propagation of the toe of the bore (see §6). Notice that, just behind the toe, two of the eigenvalues equal the two corresponding to the shallow-water equation, whereas the other two (the numerically largest) exist only behind the toe. Notice also that the maximum value of the largest eigenvalue is at the toe.

Figure 4 shows the value of the corresponding characteristic velocities for the same data as in figure 3. For reference, values of η and u_s-u_0 are shown as well. For an x/h-value around 18, the turbulence reaches the bottom and one of the equations becomes superfluous. This does represent a discontinuity in the description, and in figure 4 this is reflected by the termination of one of the characteristics.

We see that all eigenvalues are real, which indicates the hyperbolic nature of the system. It should be mentioned, however, that during the computations it was found that for the case $F_1 = 2$ two of the four eigenvalues became complex conjugate for an intermediate region of x-values if $A \gtrsim 1.85$, A being defined by (9.1). No physical interpretation has been found for this.

For $x/h \to \infty$ we have $(u, u_0) \to u_\infty$, where (see e.g. Lighthill 1978)

$$u_\infty = \frac{M^2-1}{M}\left(\frac{M^2+1}{2}\right)^{\frac{1}{2}}, \quad M \equiv \left(\frac{d_\infty}{h}\right)^{\frac{1}{2}}.$$

For the case in figure 4 this means $u_\infty = 1.156$. The eigenvalues of A similarly become

$$\left.\begin{matrix} \lambda_1, \\ \lambda_2 \end{matrix}\right\} = u_\infty \pm d_\infty^{\frac{1}{2}} = \left\{\begin{matrix} 2.696, \\ 0.384, \end{matrix}\right.$$
$$\lambda_3 = u_\infty \qquad = \ 1.156,$$

which are the asymptotic values shown in figure 4.

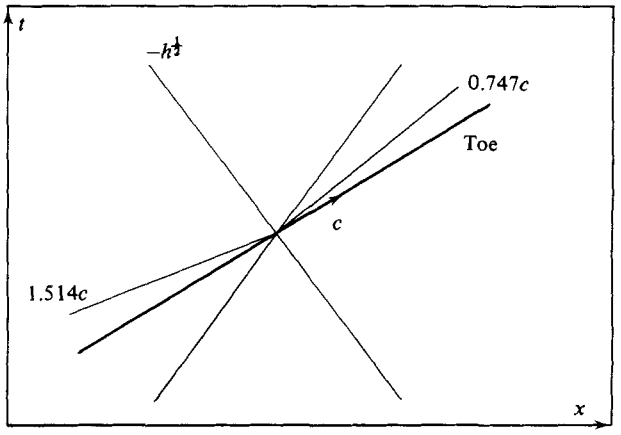

FIGURE 3. The characteristic directions at the toe of the turbulent front. The numbers correspond to the case $F_1 = c/h^{\frac{1}{2}} = 2$, and $f(\sigma)$ determined by (9.1).

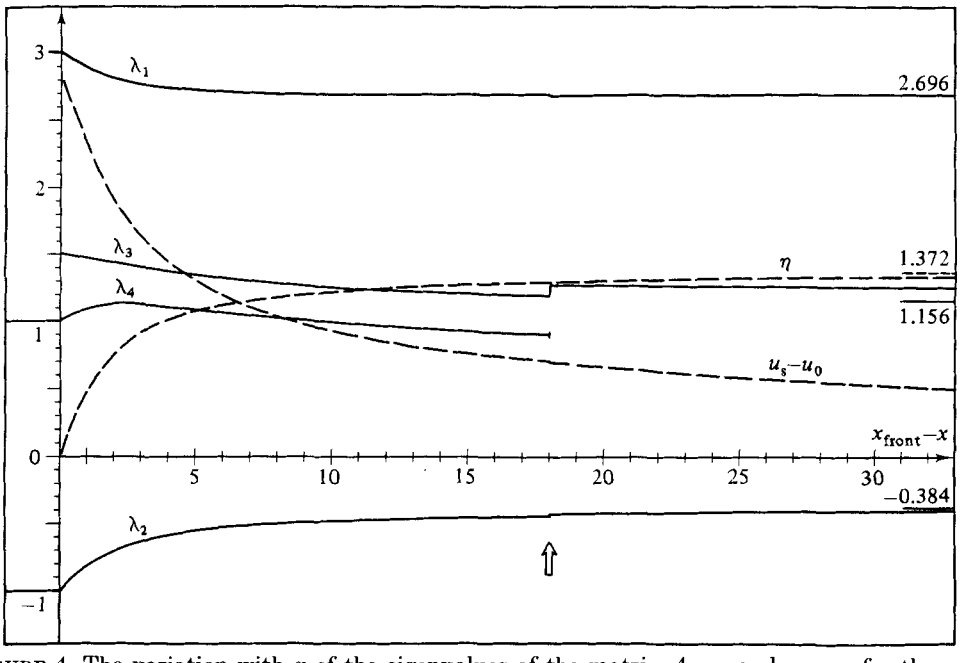

FIGURE 4. The variation with x of the eigenvalues of the matrix A_{ij}, η and $u_s - u_0$ for the same case as in figure 3. The depth is constant, and the arrow shows where turbulence reaches the bottom.

This figure also shows that the largest characteristic value $\lambda_1 = u_\infty + d_\infty^{\frac{1}{2}}$, which at infinity corresponds to the value in ordinary shocks, is not the one that at the toe is equivalent to a value in front of the toe.

It is also interesting to notice from figure 4 that we have quite appreciable differences between the surface and bottom velocities $u_s - u_0$ even at large values of x. This may be interpreted as a need for enhancing the momentum contribution in the momentum equation. This again may be combined with the observation described in I that for large x the theoretical surface elevation is somewhat smaller than the measured values, which corresponds to a momentum deficit. The accumulative effect

for large x of omitting the bottom boundary layer also influences this in both the energy and the momentum budgets.

We finally emphasize that the results obtained so far in this section are independent of the turbulence model (that is the value of $D^{(0)}$) and of the shape of $f(\sigma)$. The only assumptions required are that there *is* a similarity profile $f(\sigma)$ and that D is discontinuous at the toe. Hence we must realize that these two assumptions in fact determine the principal properties at the toe. These assumptions are further examined in §7.

7. Discussion of the flow near the toe

The flow situation in the neighbourhood of the toe is actually that of a flow separation at a free surface analysed by Longuet-Higgins (1973) (hereinafter designated II). The result (6.22), however, shows that the present model differs significantly from II. Equation (6.22) predicts a finite value of $u_s - u_0$ at the toe, and since we shall always find $S_1 > S_2$ we get

$$(u_s - u_0)^{(0)} > c \tag{7.1}$$

against $(u_s - u_0)^{(0)} = 0$ in II. Figure 5 depicts more explicitly the differences between the two models. The flow is again described in a reference frame moving with the toe of the front.

A primary difference stems from the assumption in II of a stagnation point at the toe with the velocity tending to zero both in the upper (turbulent) and in the lower flow region. In addition, the dividing streamline (defined as the streamline above which $\int u\,dz = 0$) in II forms the lower limit of the turbulent region (with $\tau \neq 0$). The present model lets the turbulence extend below the dividing streamline to get $\tau \to 0$ at the lower edge and allow for mass entrainment into the turbulent region. The latter difference, however, is of minor importance relative to the former.

From a local point of view, the assumption of a stagnation point is a very natural one, because the finite value of $u_s - u_0$ of the present model invariably leads to $\partial u/\partial z \to \infty$ as the thickness b of the turbulent region decreases towards zero at the toe. The existence of a stagnation point in the lower region must be an exception, however, since the flow in front of the toe is a potential flow. Hence, in a fixed frame of reference, to create a water-particle velocity equal to the speed c of propagation of the front (to which the existence of a stagnation point corresponds) would for a bore propagating on constant depth require accelerations corresponding to a rise in water level equal to $c^2/2g$ above the level with zero particle velocity in that reference frame. This means that in a bore the toe would always be preceded by such a rise in water level, which is not possible.

In fact, from the small to moderate rise in water level in front of the turbulent bores in the photos of figure 6 it may be inferred that the velocity u_0 immediately ahead of the toe is usually very small (in a fixed frame of reference). Even in the case of a spilling breaker in figure 6 (*c*) we get $u_0 \ll c$. Notice that the present model totally neglects this rise in water level, which in the case of a bore propagating into quiescent water will be very small. On the other hand, the surface velocity u_s in the turbulent front just behind the toe must be larger than (or at least equal to) c to prevent the turbulent region from being left behind by the propagating bore.

Hence from these considerations it is concluded that at the toe of the turbulent front the value of $u_s - u_0$ is (usually) close to c, and in any case $u_s - u_0$ will be nonzero (as suggested in the present model).

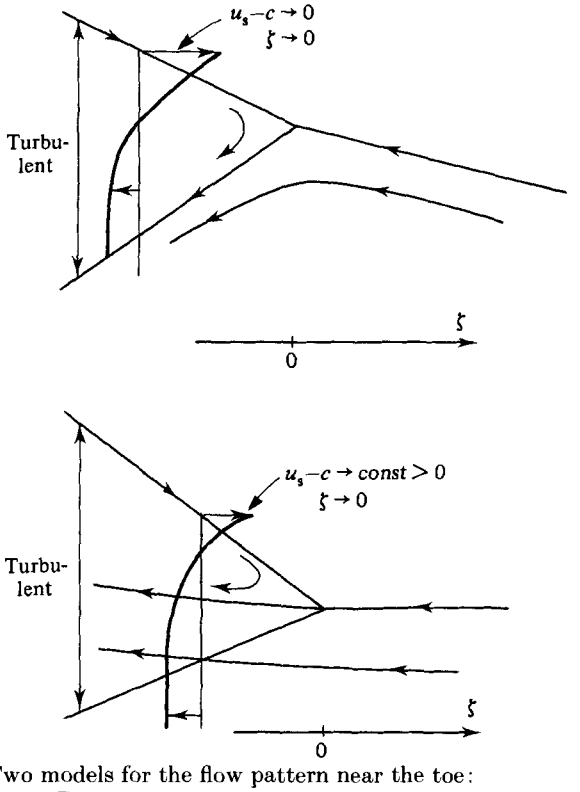

FIGURE 5. Two models for the flow pattern near the toe: (*a*) Longuet-Higgins (1973); (*b*) present theory.

If we now further assume $u(z)$ to be a continuous function of z, a non-zero value of $u_s - u_0$ implies $\partial u/\partial z \to \infty$ towards the toe, which (even in a laminar flow) would cause the shear stress τ_{zx} to increase similarly. This clearly cannot be consistent with the nearly constant value of u_s near the toe, which suggests that even $\partial \tau_{zx}/\partial z$ remains bounded.

In the present model τ_{zx} is kept finite by the form (3.8) assumed for ν_t. Notice that for the flow in the turbulent wedge (m denoting the moving reference frame) we get

$$Q_{b,\mathrm{m}} \equiv \int_b u_\mathrm{m}\,\mathrm{d}z = \int_b (u-c)\,\mathrm{d}z \approx b(u_s - u_0)\,S_1 + b(u_0 - c) \to 0 \quad \text{as} \quad \zeta \to 0, \tag{7.2}$$

which shows that the finite velocity u_s is associated with a vanishing amount of water, which is also consistent with a bounded value of the shear stress.

Finally we notice that the existence of a non-zero value of $u_s - u_0$ at the toe justifies the assumption in the last section that $D^{(0)}$ has a non-zero finite value immediately behind the toe. This can be seen by utilizing the abovementioned fact that $\partial \tau_{zx}^{(0)}/\partial z$ and hence $\tau_{zx}^{(0)}$ for physical reasons must be finite, which substituted into (2.7) yields

$$D = \int_b \tau_{zx} \frac{\partial u}{\partial z}\,\mathrm{d}z \sim b\tau_{zx}^{(0)} \frac{(u_s - u_0)^{(0)}}{b} = \tau_{zx}^{(0)}\,(u_s - u_0)^{(0)} \neq 0. \tag{7.3}$$

It should be emphasized that the above conclusions are independent of the shape $f(\sigma)$ of the velocity profile. It is not even utilized that $f(\sigma)$ is the same for all x (similarity). This implies that, although the quantitative relations derived in §6 are based on the similarity assumption, the discontinuity of $D^{(0)}$ at the toe is not.

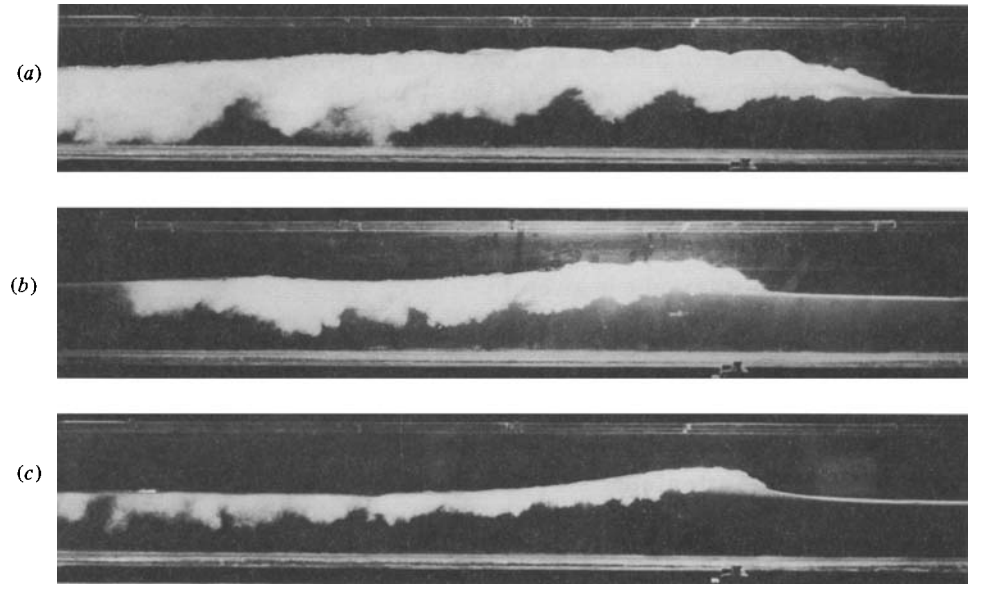

FIGURE 6. Three photos of weak bores showing the extent of the turbulent region. The photos were obtained by the following method described by Peregrine & Svendsen (1978). In a small closed-circuit flume a small amount of detergent is added to the water. The flume is operated for a while during which the pump creates numerous small bubbles only a fraction of a millimetre in diameter (rising speed less than 1 mm/s), and giving the water a milky colour. The pump is stopped and the bubbles allowed to rise to the surface. When the water has cleared, a thin layer of the small bubbles remains on the surface. When, finally, we send a bore through the flume, these bubbles are entrained into the turbulent layer and give the white colouring seen on the photos.

8. Numerical solution

The numerical scheme used in the computations is a two-step Lax–Wendroff scheme (see e.g. Richtmeyer & Morton 1967) which is of second-order accuracy. With n denoting the number of time steps each of length Δt, and i referring to computation points in the x-direction with spacing Δx, we use for (2.10) in the first of the two steps

$$V_{i+\frac{1}{2}}^{n+\frac{1}{2}} = \tfrac{1}{2}(V_i^n + V_{i+1}^n) + \tfrac{1}{2}m(F_{i+1}^n - F_i^n) + \tfrac{1}{2}m\,\Delta x(G_i^n + G_{i+1}^n), \quad m \equiv \frac{\Delta t}{\Delta x}. \tag{8.1}$$

The second step becomes

$$V_i^{n+1} = V_i^n - m(F_{i+\frac{1}{2}}^{n+\frac{1}{2}} - F_{i-\frac{1}{2}}^{n+\frac{1}{2}}) + m\,\Delta x(G_{i+\frac{1}{2}}^{n+\frac{1}{2}} + G_{i-\frac{1}{2}}^{n+\frac{1}{2}}). \tag{8.2}$$

Since a primary point of interest is to analyse the effect of adding turbulence to a bore, part of the computations were made with a bore propagating on a horizontal bottom.

In the computations with a beach, the shoreward boundary was represented by a very shallow shelf to avoid the entirely different situation of a front propagating on dry land. Hence this problem was solved essentially as an initial-value problem.

In all cases the solution for a turbulent bore of permanent form derived in I was used as starting condition seaward of the slope.

A significant difference from the dissipative Lax–Wendroff solution of the ordinary shallow-water equations is the discontinuity represented by the toe of the bore. At this point the model shifts from the ordinary shallow-water equations (i.e. (2.11)),

describing the non-turbulent flow in front of the bore, to the four-equation system derived above describing the flow in the bore itself. Hence, to determine the propagation of the bore, we must keep track of the position of the toe in each time step. The discountinuous derivatives of the dependent variables also require a one-sided difference scheme at that point.

The propagation of the toe is determined by the expression

$$\frac{\mathrm{d}x_{\mathrm{toe}}}{\mathrm{d}t} = c. \tag{8.3}$$

Here the speed of propagation c is given by

$$c = c_i = \frac{Q_x}{\eta_x} = \frac{Q_i - Q_{i-1}}{\eta_i - \eta_{i-1}}, \tag{8.4}$$

in which i is the first grid point behind the toe. Equation (8.4) is equivalent to (6.17), and hence consistent with the mathematical formulation of the problem. Physically, (8.4) implies that the instantaneous speed of propagation of the toe is determined by the flow immediately behind the toe. And, since these flow conditions are over a longer time sequence influenced by the flow structure in the entire bore, the speed of propagation of the toe, and hence of the bore itself, is in fact influenced by all points behind the toe. Mathematically, the corresponding information is carried to the toe by the fastest of the characteristics behind the front (see figure 4), which has $\mathrm{d}x/\mathrm{d}t > c$.

9. Numerical results and discussions

To obtain numerical results with the model, we must choose the velocity profile $f(\sigma)$ defined by (3.1) and the turbulence constant Ω_τ (3.8). Following I, we use for $f(\sigma)$ the cubic

$$f(\sigma) = -A\sigma^3 + (1+A)\sigma^2 \quad (0 < \sigma < 1), \tag{9.1}$$

with $A = 1.4$, and we also take

$$\Omega_\tau = \frac{0.03 S_2^2}{S_{10} S_1^2}, \tag{9.2}$$

as found in I.

Computations for a bore on a horizontal bottom verify the stability of the solution found in I for that case. These computations also show the ability of the program to propagate such a bore. Figure 7 shows a comparison between the steady profile from I with $F_1^2 = 4$ used as a boundary condition and the profile obtained after this profile has propagated 25 times the water depth.

As mentioned in §1, we see that the turbulence is stabilizing the profile in spite of the static pressure assumption. That assumption also excludes the possibility that weak bores develop into undular bores.

It may also be noticed that since we have explicitly modelled the loss of energy due to turbulence production it is important to minimize any additional numerical dissipation. This has been done by using a very fine grid (typically $\Delta x = 0.1$ h). The numerical dissipation, which is largest immediately behind the toe where the largest curvatures occur, tends to decrease the surface elevation, i.e. to flatten the profile. However, in figure 7 the numerical solution has been compared with a hydraulic-jump solution which does not contain any numerical dissipation. Clearly, the two solutions are nearly identical, indicating that the numerical dissipation is negligible in the present run. Additional evidence of this is that the results do not change by further

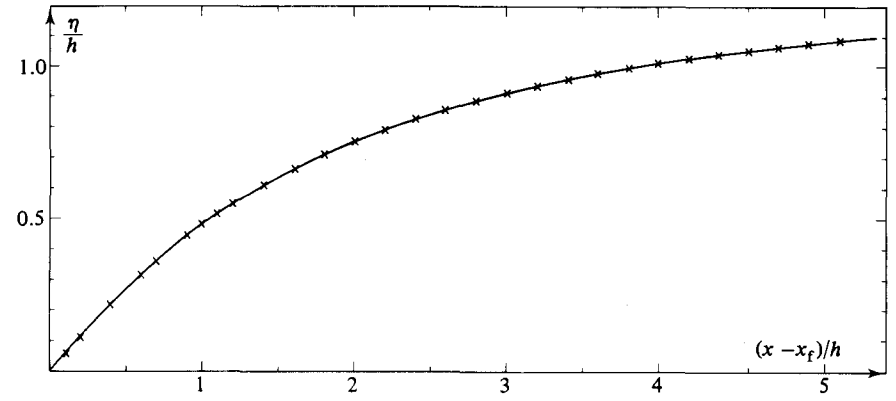

FIGURE 7. The surface profile of a bore propagating on a horizontal bottom; $F_1^2 = 4$: ——, starting profile determined from I; x, computed values after 25 water depths of propagation.

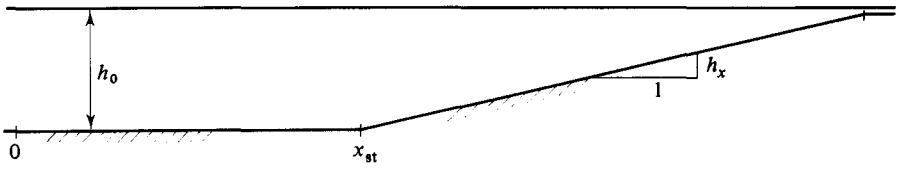

FIGURE 8. Sketch of the sloping beach.

significant reductions of Δx, which would have been the case had the numerical dissipation been noticeable.

The computation with a constant depth also shows that except for minor deviations at the start ($< 0.5\,\%$) the phase velocity equals the theoretical value of 2 within a fraction of $1\,\%$. The accuracy, however, depends somewhat on the Froude number, the smaller Froude numbers used below requiring Δx as small as $0.05h_0$. Also the Courant number C_r is of some importance, the best results being obtained with $C_r = 0.5$, based on the front speed. The value of Δt is determined accordingly at each time step.

The second group of computations were performed with a bore on a sloping bottom. Figure 8 shows the arrangement chosen, and the computations started at the edge of the slope at $x = x_{st}$. The bore is assumed to have attained the stable shape described above in the constant-depth region outside the slope.

Since there are three positive characteristics (figure 3), we can specify three boundary conditions at $x = 0$. The time variations of η, E and u_0 have been used from the steady solution. As we do not know the Riemann variables associated with the system of characteristics, the variation of Q has been determined from the other three by assuming constant form at $x = 0$.

In figure 9 is shown a comparison between the horizontal-bottom profile of figure 7 (used as input) and the profile when the toe of the front was at $h = 0.0897$. x_{st} is 18 and h_x is 0.0289. Clearly the front is less steep than the input profile, where one would perhaps expect the opposite.

An explanation for this may be found by looking at the front speed c (figure 10). c is (for this particular starting value of F_1) nearly constant, independent of the significant depth variation, which means that the value of c^2/gh (where h is the depth at the toe of the front) is increasing rapidly as the bore approaches the shoreline.

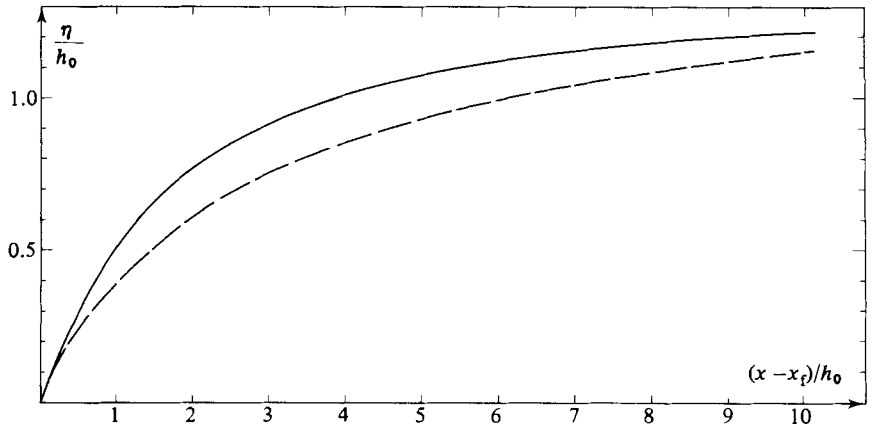

FIGURE 9. Development of the surface profile for a bore on the beach; $F_1^2 = 4$: ——, input, toe at x_{st}; – – –, toe at $h/h_0 = 0.0897$.

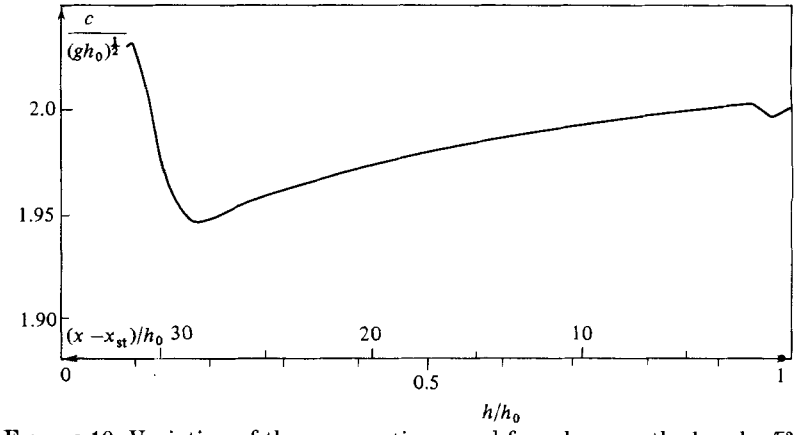

FIGURE 10. Variation of the propagation speed for a bore on the beach; $F_1^2 = 4$.

Hence, according to (6.23), we should expect $\eta^{(1)} = \eta_{x,\text{front}}$ to decrease, which is just what happens.

The value of $\eta^{(1)}$ satisfying (6.23) may not be determined from the computation points by a simple backward difference because in this context the curvature at the front is not negligible. Computations with due regard being paid to this effect show, however, that the true value of $\eta^{(1)}$ corresponds to (6.23) to within 1–2 %. In other words, for this particular example the movement of the front corresponds very closely to the first approximation derived in §6. This may not be true for steeper bottom slopes, however.

For values of c larger than $(2\text{–}3)(gh_0)^{\frac{1}{2}}$ small variations of $\eta^{(1)}$ in (6.23) imply appreciable variations in c. This in combination with the sensitivity of $\eta^{(1)}$ to the curvature of η indicates that (6.23) is unsuitable for determination of the front speed from computed values of $\eta^{(1)}$, as has already been mentioned in §6.

Also, another mechanism may contribute to this. If one thinks of a small positive perturbation being added to the toe speed, then this would for a short period cause the toe to move faster than the rest of the bore. But that would for continuity reasons decrease the surface slope $\eta^{(1)}$ just behind the toe, and so by virtue of (6.23) tend to

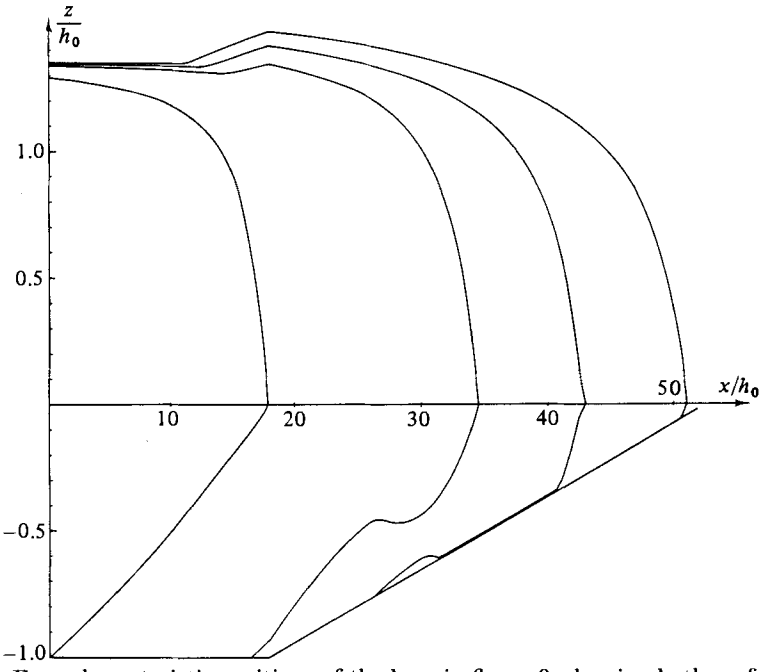

FIGURE 11. Four characteristic positions of the bore in figure 9, showing both surface profile and lower boundary of the turbulent region. The last position is at $h/h_0 = 0.0897$.

stabilize the higher propagation speed rather than damp it. Apparently, there is in this mechanism a possibility of an uncontrolled growth of c.

On the other hand, such a growth is apparently counteracted in (6.17) if $Q^{(1)}$ decreases more than $\eta^{(1)}$ when the toe moves faster.

Finally, it should be mentioned that physically (6.17) represents the continuity of mass, whereas (6.23) in essence accounts for the energy dissipation, which again indicates that c should be determined from (6.17).

Two cases for $F^2 = 4$ and 1.88 are shown in figures 11 and 12. In addition to the surface profile, the figures also show the extent of the turbulent region for the four different positions of the bore on its way towards the shoreline. The turbulent region is particularly seen to grow in thickness right behind the front as the depth increases, i.e. as the local bore strength increases, and eventually at sufficiently small depth the turbulence spreads over the whole depth from just behind the front.

Another characteristic feature is that the height of the front stays nearly constant even though the steepness near the toe decreases as figure 10 showed.

It may also be noticed that, as the bore propagates, the turbulence at a given x-position slowly spreads towards the bottom, a feature of the computations which is quite in accordance with physical observations. The small 'bubble' on the bottom shows a short interval where the equations require turbulence to cover less than the full depth.

From computations with larger values of Δx it was found that the surface profile is quite insensitive to such changes. The most variable quantity in the results is b, the height of the turbulent region. For the value of 0.05 for Δx used in these computations only small changes in b will occur by an increase of 50 % in Δx.

Computations have also been made for comparison with the dissipative Lax–Wendroff scheme used by Hibberd (1977) and Hibberd & Peregrine (1979). A direct comparison between the profiles is not really informative, however.

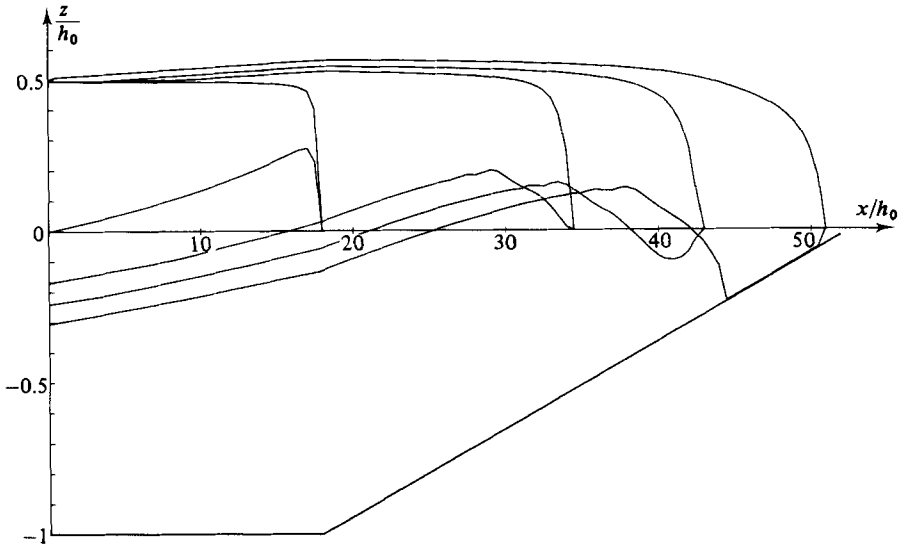

FIGURE 12. Four characteristic positions equivalent to figure 11 for $F_1^2 = 1.88$.

One reason is that using the Lax–Wendroff scheme the length of the front is artificially fixed to cover 4–5 computation points, so that it is determined by the choice of Δx. Hence the front shape is unphysical in such computations. Another reason is that the boundary conditions at the seaward boundary are different in the two investigations.

Hibberd & Peregrine use a boundary condition that in a linear approximation absorbs the (small) reflection from the shore, whereas in the present investigation the constant-form assumption mentioned above implies reflection with a sign shift of the (weak) outgoing waves.

Since the latter difference has only a minor effect on the shape of the fronts, however, it is relevant to compare the front speeds. Figure 13 shows such a comparison for $F^2 = 1.88$. The propagation velocity for the Lax–Wendroff method has been obtained from Hibberd (1977) assuming a constant form of the front so that $c = ud/\eta$. Simultaneous values of u, d and η at the crest immediately behind the front have been used.

The Hibberd bore is seen to propagate at a speed approximately equal to that of a bore on a constant depth having the same height as the front height (determined by estimating the average of the undulations created by the numerical scheme) and at the depth of the front (the difference being within the range of uncertainty of the results available).

On the other hand, our front toe starts with nearly the same speed as the Hibberd bore (actually slightly less because of the initial deformation of the Hibberd bore), but as the front becomes less and less steep the toe moves increasingly faster than the Hibberd bore, with a value about 10% higher being typical near the shoreline. For both methods, however, the propagation velocity decreases with the decreasing depth, in which sense this case differs from the results for $F_1^2 = 4$ (see figure 10).

The propagation speeds larger than the bore speed can only be associated with an enhancement (relative to a stable, constant depth bore) of the momentum flux behind the toe due to the non-uniform velocity profiles. No measurements are known to the authors for bores, but a more detailed discussion of the mechanisms is given in Svendsen, Madsen & Buhr Hansen (1978).

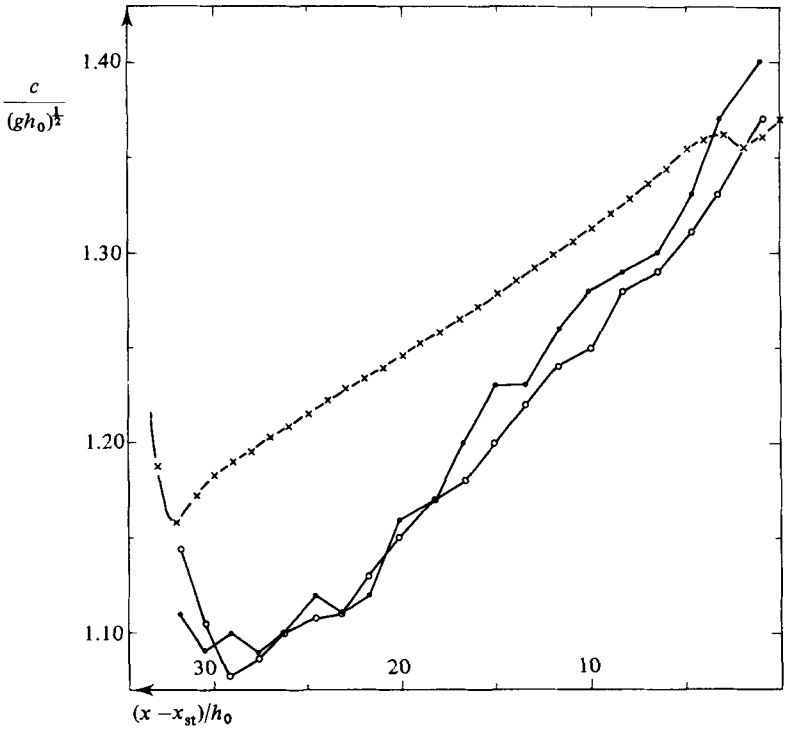

FIGURE 13. The propagation velocities for the case $F_1^2 = 1.88$: ●, derived from Hibberd's results; ○, a bore with height equal to the front height in Hibberd's computations; ×, our computations.

10. Concluding remarks

The aim of the reported work has been to investigate how a turbulent bore develops on a beach.

The turbulence is modelled the same way as in Madsen & Svendsen (1983) and the same assumptions are used for the velocity and pressure distributions. The equations, however, in this propagation model are simultaneous partial differential equations of hyperbolic type (instead of the primary algebraic equations in Madsen & Svendsen).

The most important detail of the flow is at the toe of the turbulent front, and it is found that the description gives qualitatively the correct variation of the crucial physical quantities. A numerical check using the steady-state solution found in Madsen & Svendsen as input also shows that on a constant depth this solution does propagate without change of form.

Finally, results are given for two bores climbing a beach, and the speed of propagation is compared with similar results obtained by Hibberd & Peregrine using a dissipative Lax–Wendroff scheme. It is found that the latter moves at a somewhat lower speed, the difference increasing towards the shoreline.

Since more details of the flow are determined, the present method will computationally be less economical than the Lax–Wendroff scheme for the shallow-water equations. On the other hand, no attempt has been made here to optimize the numerical computations, and often we have chosen smaller grid sizes for the results than necessary. And with modern computers the computation effort required is rather modest.

The authors are grateful to acknowledge the support from the Danish Council for Scientific and Industrial Research.

REFERENCES

BENJAMIN, T. B. & LIGHTHILL, M. J. 1954 On cnoidal waves and bores. *Proc. R. Soc. Lond.* A **224**, 448–460.

BÜRGER, W. 1967 A note on the breaking of waves on non-uniformly sloping beaches. *J. Math. & Mech.* **16**, 10.

HIBBERD, S. 1977 Surf and run-up. Ph.D. thesis, University of Bristol.

HIBBERD, S. & PEREGRINE, D. H. 1979 Surf and run-up on a beach: a uniform bore. *J. Fluid Mech.* **95**, 323–345.

HINZE, J. O. 1959 *Turbulence.* McGraw-Hill (2nd edn 1975).

JEFFREY, A. 1964 The breaking of waves on a sloping beach. *Z. angew. Math. Phys.* **15**, 97–106.

JEFFREY, A. & MVUNGI, J. 1980 On the breaking of water waves in a channel of arbitrarily varying depth and width. *Z. angew. Math. Phys.* **31**, 758–761.

KELLER, H. B., LEVINE, D. A. & WHITHAM, G. B. 1960 Motion of a bore over a sloping beach. *J. Fluid Mech.* **7**, 302–316.

LAUNDER, B. E. & SPALDING, D. B. 1972 *Mathematical Models of Turbulence.* Academic.

LAX, P. D. & WENDROFF, B. 1960 Systems of conservation laws. *Commun. Pure Appl. Maths* **13**, 217–237.

LIGHTHILL, J. 1978 *Waves in Fluids.* Cambridge University Press.

LONGUET-HIGGINS, M. S. 1973 A model of flow separation at a free surface. *J. Fluid Mech.* **57**, 129–148.

MADSEN, P. A. & SVENDSEN, I. A. 1983 Turbulent bores and hydraulic jumps. *J. Fluid Mech.* **129**, 1–25.

MEYER, R. E. & TAYLOR, A. D. 1972 Run-up on beaches. In *Waves on Beaches and Resulting Sediment Transport* (ed. R. E. Meyer), pp. 357–411. Academic.

PACKWOOD, A. R. 1980 Surf and run-up on beaches. Ph.D. thesis, University of Bristol.

PACKWOOD, A. R. & PEREGRINE, D. H. 1981 Surf and run-up on beaches: models of viscous effects. *Univ. Bristol Rep.* AM-81-07.

PEREGRINE, D. H. 1966 Development of an undular bore. *J. Fluid Mech.* **25**, 321–330.

PEREGRINE, D. H. 1972 Equations for water waves and the approximations behind them. In *Waves on Beaches and Resulting Sediment Transport* (ed. R. E. Meyer). Academic.

PEREGRINE, D. H. & SVENDSEN, I. A. 1978 Spilling breakers, bores and hydraulic jumps. In *Proc. 16th Coastal Engng Conf., Hamburg*, vol. I, pp. 540–550.

RICHTMYER, R. D. & MORTON, K. W. 1967 *Difference Methods for Initial-Value Problems.* Interscience.

SHEN, M. C. & MEYER, R. E. 1963 Climb of a bore on a beach. Part 2. Non-uniform beach slope. *J. Fluid Mech.* **16**, 108–112.

STIVE, M. J. F. & WIND, H. G. 1982 A study of radiation stress and set up in the near-shore region. *Coastal Engng* **6**, 1–26.

SVENDSEN, I. A., MADSEN, P. A. & BUHR HANSEN, J. 1978 Wave characteristics in the surf zone. In *Proc. 16th Coastal Engng Conf., Hamburg*, vol. I, pp. 520–539.

WHITHAM, G. B. 1958 On the propagation of shock waves through regions of non-uniform area or flow. *J. Fluid Mech.* **4**, 337–360.

WHITHAM, G. B. 1974 *Linear and Nonlinear Waves.* Wiley.

WILKINSON, D. L. & BANNER, M. L. 1977 Undular bores. In *Proc. 6th Australasian Hydraul. and Fluid Mech. Conf., Adelaide*, pp. 369–373.